

Article

# Super-Lattice Structure and Phase Evolution of $\text{Pb}(\text{Lu}_{0.5}\text{Nb}_{0.5})\text{O}_3\text{-PbTiO}_3$ Single Crystal with Low $\text{PbTiO}_3$

Ying Liu, Xiaoming Yang, Chao He \* , Xiuzhi Li, Zujian Wang and Xifa Long \*

Key Laboratory of Optoelectronic Materials Chemistry and Physics, Fujian Institute of Research on the Structure of Matter, Chinese Academy of Sciences, Fuzhou 350002, China; liuying@fjirsm.ac.cn (Y.L.); xmyang@fjirsm.ac.cn (X.Y.); lxz@fjirsm.ac.cn (X.L.); wangzujian@fjirsm.ac.cn (Z.W.)

\* Correspondence: hechao@fjirsm.ac.cn (C.H.); lxf@fjirsm.ac.cn (X.L.)

Received: 29 November 2017; Accepted: 20 January 2018; Published: 23 January 2018

**Abstract:** The phase diagram of the  $\text{Pb}(\text{Lu}_{0.5}\text{Nb}_{0.5})\text{O}_3\text{-PbTiO}_3$  (PLN-PT) binary system was previously reported based on XRD and dielectric measurements results. Unusually, the Curie temperature of PLN-PT with low PT obtained from the phase diagram is much lower than that of PLN and PT end members, which is different from others, such as PZT. Therefore, the complex structure of PLN-PT with low PT is desired to be studied. In this work, PLN-PT single crystals with low PT were grown for the study of their super-lattice structure and phase evolution. The super-lattice reflections were identified by X-ray diffraction. Domains and their evolution by heating from room temperature to 150 °C were observed under a polarized light microscope. The phase transition from the ferroelectric phase to the paraelectric phase was determined by dielectric spectra and polarized light microscopy. A precursor/intermediate phase exhibiting pinched hysteresis loops was displayed above the Curie temperature, which originates from some polar region embedded in the non-polar matrix. The coexistence of the ferroelectric and antiferroelectric domains leads to peculiarities of the phase transitions, such as a lower Curie temperature compared with PLN and PT. The studies of the phase evolution of PLN-PT with low PT single crystal is a supplementary amendment of the PLN-PT phase diagram as previously reported.

**Keywords:** antiferroelectric; super-lattice; phase diagram; single crystals

## 1. Introduction

An antiferroelectric (AFE) state is defined as one in which lines of ions are spontaneously polarized but with neighboring lines polarized in antiparallel directions [1]. In other words, antiferroelectricity is revealed by the antiparallel displacements of  $\text{Pb}^{2+}$  ions and the B-site atom ordering in lead-based perovskite materials [2], and has wide applications in energy storage capacitors, mobile electronic devices, and explosive electrical transducers [3–5]. As an important member of perovskite structure AFEs,  $\text{Pb}(\text{Lu}_{0.5}\text{Nb}_{0.5})\text{O}_3$  (PLN) ceramics were first reported by Kupriyanov and Isupov in the early 1960s [6,7]. The structure and AFE properties of PLN single crystals were studied in our laboratory [2]. Two sets of superlattice reflections, including the B-site atom ordering type reflection and the lead-ion antiparallel ordering type reflection, coexist in PLN single crystals. The Curie temperature  $T_C$  of PLN was about 240 °C and 254 °C for [111]-oriented and [001]-oriented crystal plates, respectively. The value of the energy density was calculated to be 3.65 J cm<sup>-3</sup> for the [111]-oriented sample at 200 °C based on double hysteresis loops with an electric field  $E_{\text{APP}} = 170 \text{ kV cm}^{-1}$  applied.

One of the usual methods for modifying lead-based perovskite AFE materials is the addition of other elements, including for achieving low PT [8,9]. PLN-PT ceramics have been investigated in the past few years. M. Antonova et al. reported a  $(1-x)\text{PLN-xPT}$  ceramics system obtained by

solid phase reactions with subsequent hot pressing [10]. The compositions within the morphotropic phase boundary (MPB) region (the PT content  $x = 0.38 - 0.49$ ) show a high Curie temperature ( $T_c > 350$  °C) and a large electromechanical coupling factor ( $k_p = 0.66$ ,  $k_t = 0.48$ ) for 0.59PLN-0.41PT [11]. The  $(1 - x)$ PLN- $x$ PT ceramics were also studied by D. Shen et al. in our lab with a re-modified MPB region of  $x = 0.48 - 0.50$ . The Curie temperature was up to 375 °C ( $x = 0.48$ ) and showed good piezoelectric properties ( $d_{33} = 350$  55pC/N) [12]. The high Curie temperature and good piezoelectric properties of the PLN-PT system imply that a PLN-PT single crystal can be a promising good piezoelectric material; therefore, a series of PLN-PT binary ferroelectric (FE) crystals has been successfully obtained by a top-seed solution growth technique in our lab. The crystals reveal an MPB ( $x = 0.49 - 0.51$ ) and the composition  $x = 0.49$  shows a high Curie temperature ( $T_c = 360$  °C) and high piezoelectric properties ( $d_{33} = 1630$  pC/N) [13–15].

According to Antonova's report, the  $(1-x)$ PLN- $x$ PT ceramic system transforms from pseudomonoclinic (space group Bmm2) to tetragonal (space group P4mm) at room temperature [11]. However, by Shen's report, the phase structure at room temperature changes from rhombohedral (space group R3m) to tetragonal (space group P4mm) [12]. Recently, we studied the typical relaxor behavior in compositions of  $x = 0.281, 0.328, 0.423$ , and  $0.446$ , where only the rhombohedral phase was confirmed [14]. However, it was found that the symmetry of the relaxors ferroelectric (FE) PLN-0.2PT and AFE PLN were orthorhombic [15]. The phase diagram of the PLN-PT binary system was previously reported based on XRD and dielectric measurements results [13]. Unusually, some peculiarities of the PLN-0.07PT system have been observed, such as that the Curie temperature of PLN-PT with low PT obtained from the phase diagram is much lower than that of PLN and PT end members. It is observed that in  $x = 0.1$  and  $0.2$  of  $(1-x)$ PLN- $x$ PT ceramics [11] and  $0 < x < 0.33$  of  $(1-x)$ PLN- $x$ PT crystals [13] the temperature of the dielectric anomaly deviates from the ideal linear relationship between 240 °C (PLN) and 490 °C (PT). Compared with the typical  $\text{Pb}(\text{Zr}_{1-x}\text{Ti}_x)\text{O}_3$  system, the PZT with low PT content ( $x < 0.05$ ) are AFEs at room temperature, AFE–FE phase-transition regions exist, and the Curie temperature is between that of the PZ and PT content [16]. Therefore, we think there would be another line missing in the  $(1-x)$ PLN- $x$ PT phase diagram [13]. The existence of such a region requires more detailed targeting investigations, which are also a direction of our follow-up work, and we are in the process of studying it, including in this work. If the transition is second-order, the dielectric constant will be continuous and nearly constant with temperature at the Curie point [2], so that we may lose sight of some details from the dielectric spectra. Additionally, the investigation on AFE PLN-PT single crystals with low PT can help us to understand not only the physics and chemistry phenomena of the binary AFE system, but also the way to improve the potential applications of AFE PLN-based single crystal. In this paper, we report the super-lattice structure and phase evolution behavior of PLN-0.07PT single crystal.

## 2. Experiment Section

PLN-0.07PT single crystals were successfully grown by the top-seeded solid solution growth (TSSG) method with good quality and high compositional homogeneity by means of adding flux to decrease the growing temperature. The starting chemicals, PbO (99.9%), TiO<sub>2</sub> (99.9%), Lu<sub>2</sub>O<sub>3</sub> (99.99%), Nb<sub>2</sub>O<sub>5</sub> (99.9%), and H<sub>3</sub>BO<sub>3</sub> (99.9%), were weighed according to the formula  $(1-x)$ PLN- $x$ PT ( $x = 0.2$ ). The detailed growth process and the proper flux-to-solute molar ratio were described in an earlier paper of PLN-PT crystals growth [13–15]. Finally, the single crystal has been obtained as shown in Figure 1.

The actual chemical compositions of the grown crystal were determined to be  $x = 0.07$  (PLN-0.07PT) by inductively coupled plasma atomic emission spectroscopy (ICP-AES, JY Ultima-2, Longjumeau Cedex, France). The phase and structure of the grown crystal were examined by X-ray diffractometer using *Cu-K $\alpha$*  radiation (*Miniflex600*, Rigaku, Tokyo, Japan) at room temperature. The temperature dependence of the powder X-ray diffraction was determined by another X-ray diffractometer (*Ultima IV*, Rigaku, Tokyo, Japan). The peaks were scanned continuously in  $2\theta$  steps

of  $0.02^\circ$ , with an angular range of  $10\text{--}80^\circ$  and a rotating speed of  $5^\circ/\text{min}$ . Fine crystal powder for the electron microscopy study was polished mechanically and measured on a transmission electron microscope (TEM) (*Tecnai F20 FEG*, FEI, Hillsboro, OR, USA). A polarized light microscope (*Axio Scope. A1*, Carl Zeiss, Gottingen, Germany) was employed to determine the domain structure and its evolution versus the different temperatures. For electrical properties characterization, plate was sliced from the as-grown crystal along the  $[111]$  direction, then the sample was polished and coated with silver paste as electrodes. Measurements of the dielectric constant and loss tangent ( $\tan\delta$ ) were carried out by a computer-controlled Alpha-broadband dielectric/impedance spectrometer (Novocontrol GmbH, Montabaur, Germany) with an alternating current (AC) signal of 1.0 V (peak-to-peak) applied. Polarization-electric field hysteresis loops were displayed by a standard ferroelectric test system (TF Analyzer 2000E, *aix-ACCT*, Aachen, Germany) combined with a high-voltage supply amplifier/controller (*Model 610E*, Trek, Medina, NY, USA) and an environmental test chamber (*DELTA 9023*, Delta Design, Poway, CA, USA) with temperature variations from room temperature up to  $220^\circ\text{C}$ .



**Figure 1.** As-grown PLN-0.07PT crystal using the top-seeded solid solution growth (TSSG) method.

### 3. Results

A photograph of the obtained PLN-0.07PT crystal is shown in Figure 1. The external macro structure of the crystal is a tetrakaidecahedron combination with pseudocubic (100) and (111) planes in habit, and the crystal is a light yellow color. The dimensions of the largest single crystal block generally reach  $9 \times 15 \times 13 \text{ mm}^3$  in size. At room temperature, the X-ray diffraction pattern of PLN-0.07PT exhibits a typical perovskite structure as shown in Figure 2. In addition, some super-lattice reflections, which originate from long-range ordering of B-site cations, can also be seen. The presence of a super-lattice reflection suggests that the prototypical crystal structure is an ordered perovskite with an effective unit cell that is  $(2a_c \times 2a_c \times 2a_c)$  doubled in size in all crystallographic axis directions of a cubic, simple perovskite cell ( $a_c \times a_c \times a_c$ ). Here, the subscript “c” refers to the cubic perovskite basis cell [4]. PLN-0.07PT exhibits a number of super-lattice peaks, with some of the obvious peaks corresponding to d-spacing values twice as much as those of  $(111)_C$ ,  $(311)_C$ ,  $(331)_C$ ,  $(333)_C$ ,  $(511)_C$ , and  $(531)_C$ , while major ones can be indexed as  $1/2(111)_C$ ,  $1/2(311)_C$ ,  $1/2(331)_C$ ,  $1/2(333)_C$ ,  $1/2(511)_C$ , and  $1/2(531)_C$ , respectively, showing the good-order feature of a single crystal. Special attention was focused on the  $(200)_C$  peak. It is known that the XRD profiles of  $(200)_C$  reflections in the orthorhombic (O) phase would split into three peaks: the  $O(200)$ ,  $O(020)$ , and  $O(002)$  profiles [17]. The  $O(002)$  and  $O(020)$  peaks are so closed that the intensity of the  $O(002)/(020)$  peak is twice as that of the  $O(200)$  peak. As evidenced from the split in the fundamental lines around  $2\theta \approx 43.4\text{--}44.0^\circ$  at room temperature, shown in the insets of Figure 2, the lattice distortion is found to be orthorhombic in nature.

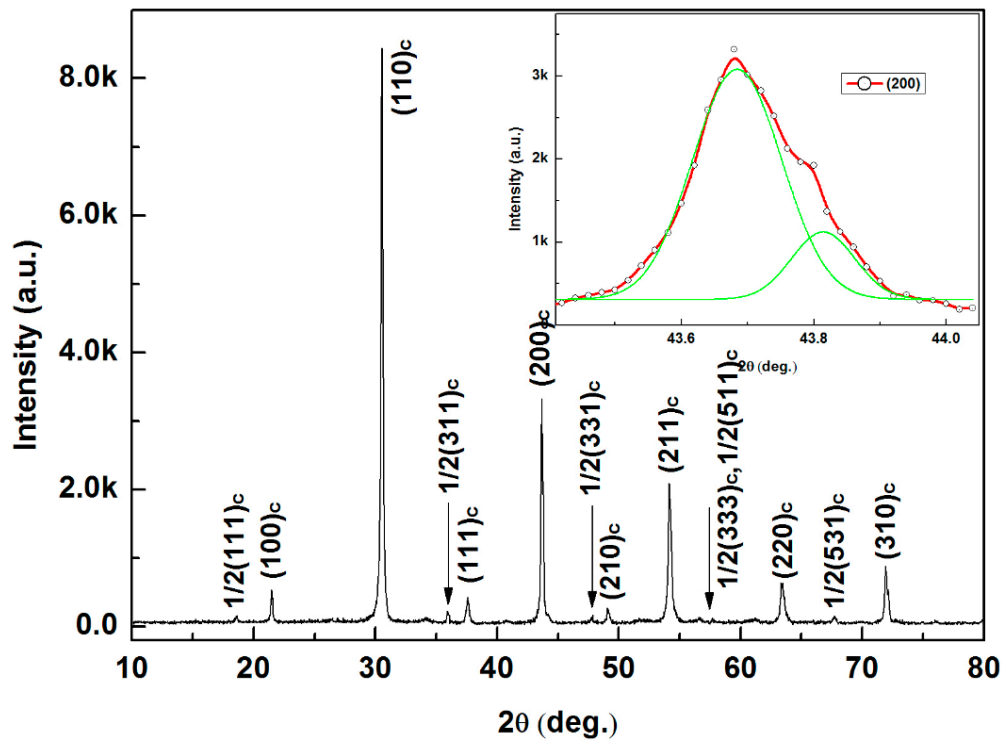


**Figure 2.** X-ray powder diffraction patterns of the crashed PLN-0.07PT crystal. The insert shows the  $(200)_c$  peak detail reflections which were fitted by the Gaussian functions.

The super-lattice reflections were further identified by transmission electron microscopy as shown in Figure 3a. The pattern in Figure 3a is composed of the fundamental spots of the prototype (the large bright spot) and the extra B-site atom ordering super-lattice reflection spots (the small dark spot), corresponding to  $1/2(111)$  and others. Micro-domains configurations in the PLN-0.07PT crystal were also studied using TEM, which were clearly found and were 1~2 nm in size as shown in Figure 3b.

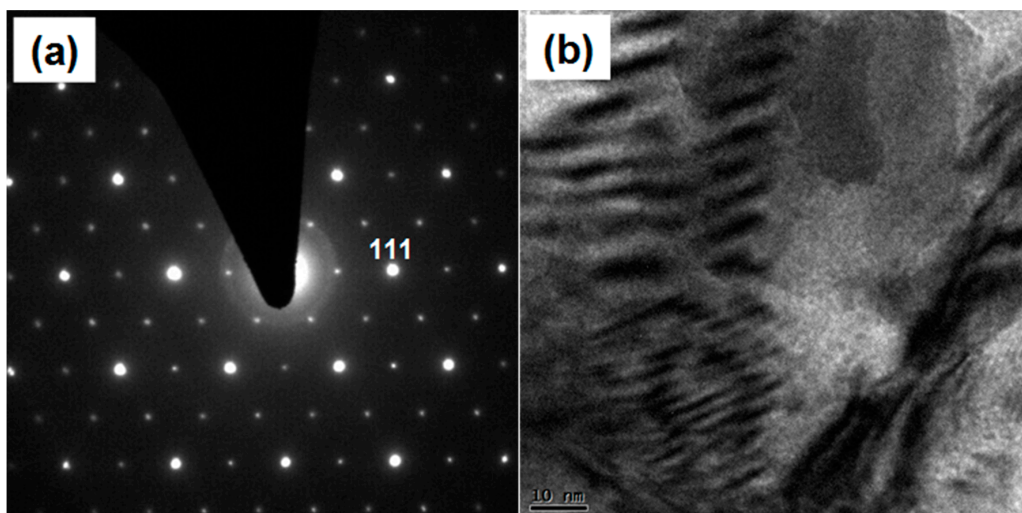


**Figure 3.** (a) Electron diffraction patterns of PLN-0.07PT single crystals exhibiting super-lattice reflections and (b) micro-domains configurations under TEM.

The macro-domain structures of the  $[111]$ -oriented plate of the PLN-0.07PT crystals were investigated under a crossed polarized light microscope as shown in Figure 4. The domains appear to

be in extinction or full bright locally based on the direction of polarization and the polarizer. As shown in Figure 4, the domains appear to be in extinction when  $\theta = 0^\circ$  ( $\theta$  is defined as the smaller angle between the  $[110]$  crystallographic axis and the polarizer), while the field manifests full bright when the objective table was rotated  $45^\circ$ , further confirming the orthorhombic symmetry of the PLN-0.07PT crystal at room temperature. The evolution of the domain is studied under a crossed polarized light microscope by heating from room temperature to  $150^\circ\text{C}$  as shown in Figure 5. Few changes are observed below  $130^\circ\text{C}$ . By continuous heating, some bright parts of the domains started to disappear until they disappeared completely at  $150^\circ\text{C}$ . It is indicated that a phase transition of the crystal occurred between  $130^\circ\text{C}$  and  $140^\circ\text{C}$ , which will be discussed hereafter.

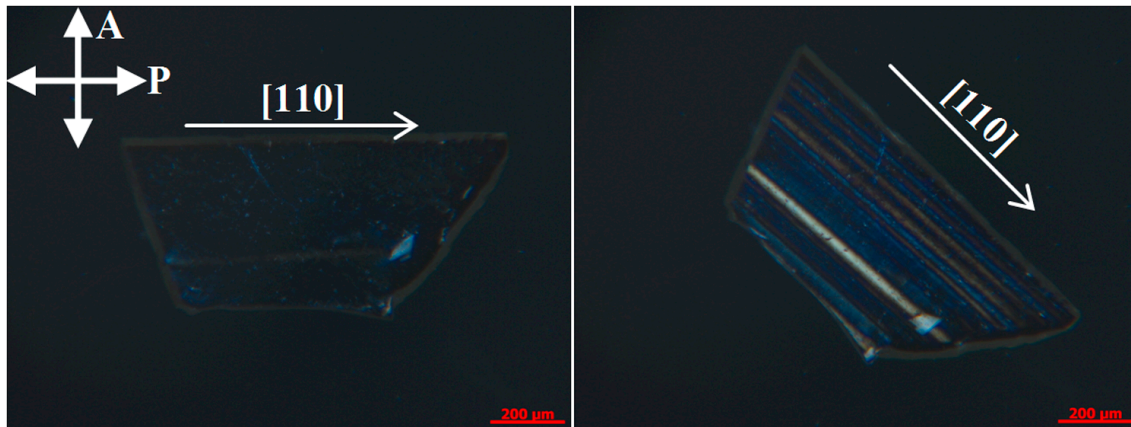


**Figure 4.** Micrographs of  $[111]$ -oriented plates of PLN-0.07PT crystal under a crossed polarized light microscope (shown by arrows) at room temperature.

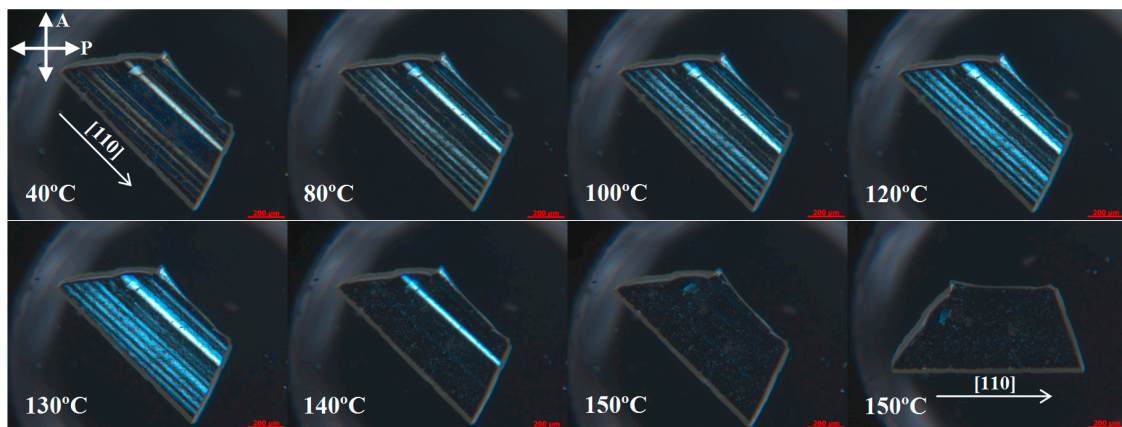


**Figure 5.** Temperature dependence of  $[111]$ -oriented plates of PLN-0.07PT crystal under a crossed polarized light microscope.

Figure 6 shows the temperature dependence of the dielectric constant  $\epsilon'$  and loss tangent  $\tan\delta$  at various frequencies for unpoled  $[111]$ -oriented crystal plates. The room temperature values of the dielectric constant and loss tangent at 1 kHz are 337 and 0.03, respectively. The behavior at a low value of  $\epsilon'$  is like most AFE materials. It shows a sharp peak at  $T_{max} = 125^\circ\text{C}$  (1000 Hz), indicating ferroelectric–paraelectric phase transition, i.e., Curie temperature  $T_C$ . No obvious frequency dispersion is found near  $T_{max}$ , indicating normal ferroelectric behavior.

The polarization-electric field ( $P$ - $E$ ) hysteresis loops of a  $[111]$ -oriented PLN-0.07PT crystal platelet at various temperatures under a bipolar drive of  $E = \pm 100\text{ kV/cm}$  at 2 Hz is shown in Figure 7. It is found that the PLN-0.07PT crystal exhibits saturated single hysteresis loops at temperatures below

130 °C, which is the meaning of the FE state. With the increasing of temperature, the FE hysteresis loops are transformed into double hysteresis loops (some displayed as pinched hysteresis loops). The double hysteresis loops disappear between 170 °C and 180 °C, which is approximately 45 °C above the Curie temperature  $T_C$ .

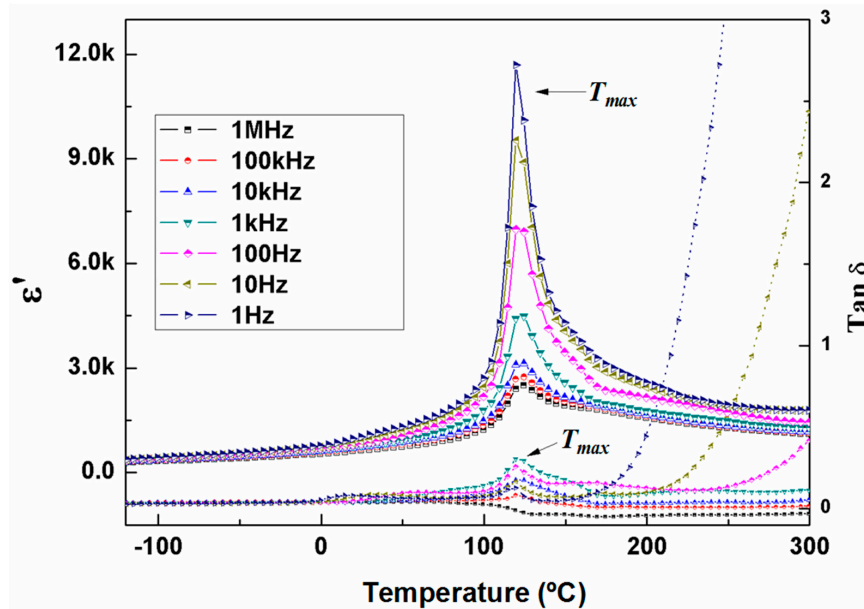


**Figure 6.** The temperature dependence of the dielectric constant ( $\epsilon'$ ) and the loss tangent ( $\tan\delta$ ) at various frequencies for unpoled [111]-oriented plates.

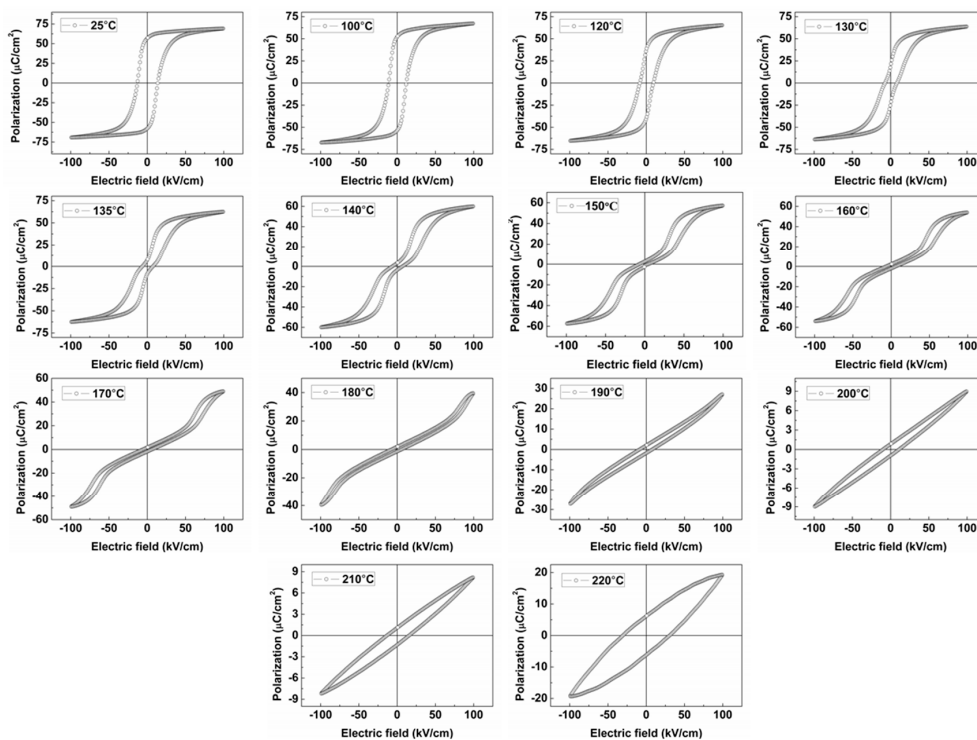


**Figure 7.** Polarization versus electric field ( $P$ - $E$ ) loops for the [111]-oriented plates of PLN-0.07PT crystal at various temperatures ( $f = 2$  Hz).

#### 4. Discussion

Surprisingly, the PLN-0.07PT single crystals exhibit some peculiarities. One feature is that the Curie temperature (125 °C) obtained from the temperature dependence of the dielectric constant is a little lower than the temperature of the phase transition from FE hysteresis loops to double hysteresis loops (130–140 °C) and the temperature of disappearance of the domain as shown in Figure 5 (140 °C), indicating non-centrosymmetric regions above  $T_C$ . It is clearly seen that the double hysteresis loops disappear between 170 °C and 180 °C as shown in Figure 7, which is much higher than the Curie temperature. It is commonly believed that double hysteresis loops above the Curie temperature should be considered pinched hysteresis loops because there exist a region with some polar regions embedded in the non-polar matrix. This kind of double hysteresis loop has been found in various materials, such as  $\text{Pb}(\text{Zr,Ti})\text{O}_3$  [18],  $\text{BiFeO}_3$  [19], and  $\text{BaTiO}_3$  [20]. In these system, some types of inhomogeneity, structural disorder, and structural defects with local polarity are present in these materials, leading to the domain walls being strongly pinned by defects [18,19]. In addition, pinched hysteresis loops exhibit a small polarization for a zero electric field. The remnant polarizations  $P_r$  of PLN-0.07PT crystals down to not zero (the value of  $P_r$  at 170 °C and 180 °C is 1.39 and 1.28  $\mu\text{C}/\text{cm}^2$ , respectively) with the increasing of temperature, indicating a pinched hysteresis loops. The above analysis means that a precursor/intermediate state (125–170 °C) exhibiting pinched hysteresis loops is displayed above the Curie temperature. These pinched hysteresis loops possessing electric dipoles are intrinsic in nature and can also occur in defect-free systems, such as  $\text{BiFeO}_3$  [21].

Another peculiar feature is that the Curie temperature of PLN-0.07PT is much lower than that of PLN (258 °C) and PT (490 °C) [13]. This peculiarity in the PLN-0.07PT system is related to the coexistence of the domains of the FE and AFE phases in a wide temperature range. First, Figure 2 shows some super-lattice reflections which originate from long-range ordering of B-site cations, suggesting the existence of AFE phase. In addition, the B-site atom ordering super-lattice reflection spots are also observed using transmission electron microscopy as shown in Figure 3. However, typical and saturated FE hysteresis loops are observed below 130 °C as shown in Figure 7. Therefore, the main body of the phase is the FE phase at room temperature. This indicates the coexistence of the domains of the FE and AFE phases in the PLN-0.07PT system. In consideration of the intermediate state, it is also reasonable that the domains of the FE and AFE phases coexist in a wide temperature range. This state of affairs leads to the fact that the free energies of both ordered states differ little. The presence of a phase transition between the FE and AFE states at a small difference in the free energies of the phases (over a wide temperature range) leads to the coexistence of the domains of these phases and the peculiarities of phase transitions, such as the lower Curie temperature compared with PLN and PT.

It is well-known that a dielectric constant with a sharp peak could fit the Curie–Weiss law ( $1/\epsilon' = (T - T_{CW})/C$ , where  $C$  is the Curie constant and  $T_{CW}$  is the Curie–Weiss temperature) very well above the Curie temperature. Figure 8 shows the fitting of the Curie–Weiss law of PLN-0.07PT single crystals (1000 Hz). Interestingly, the two sections ( $T_1 - T_2$ ,  $T_2 - T_3$ ) of the reciprocal of the dielectric constant can be fitted with the Curie–Weiss law, respectively. The values of  $T_1$ ,  $T_2$ , and  $T_3$  are about 125, 170, and 280 °C, respectively. The FE–PE phase transition exhibits a normal phase transition ( $T_1 = T_{max} = T_C$ ). It is reported that the polar regions (clusters) grow when approaching  $T_C$  from the high-temperature side, reaching several lattice constants at the temperature  $T_{PR} = 1.1 * T_C$  (K) [22,23]. For PLN-0.07PT single crystals, the value of  $T_C$  is 398 K (125 °C). The temperature  $T_{PR}$  is 437.8 K ( $1.1 \times 398 \text{ K} = 437.8 \text{ K}$ ). This value is close to the value of  $T_2$  (443 K). This points out that the polar region will induce anomalous behaviors in the temperature range from 443 K (170 °C), such as pinched hysteresis loops.

In order to confirm the structure phase transition of PLN-0.07PT single crystals, the temperature dependence of the structure was examined by XRD as shown in Figure 9. It can be seen that the peaks of  $(200)_C$  (“C” refers to the cubic phase) reflections (shown in the inset of Figure 9) shift to a high angle ( $2\theta$ ) at 160 °C, indicating that a structure transition occurred between 100 °C and 160 °C, which corresponds to the FE–PE phase transition. Then, the  $2\theta$  shifts to a low angle with an increasing

of temperature to 350 °C, which is induced by the disappearance of local non-centrosymmetric polar regions. Note that the symmetry of PLN-0.07PT single crystals at the PE phase is orthorhombic. Of course, the determination of the accurate temperature of a phase transition requires more work, such as the measurement of the loops accompanied by X-ray measurements in the field.

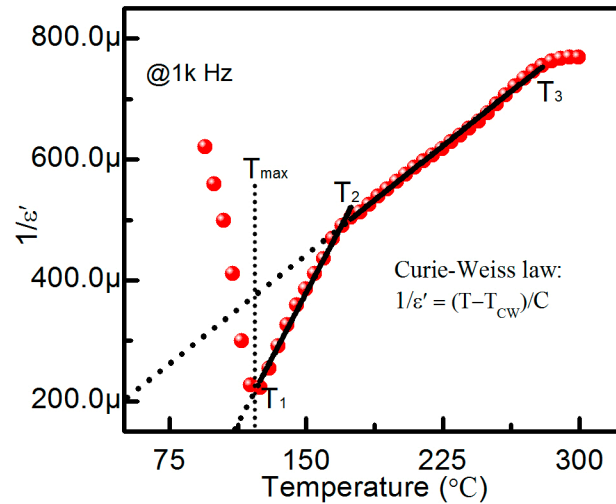


**Figure 8.** The fitting of the Curie–Weiss law of PLN-0.07PT single crystals.

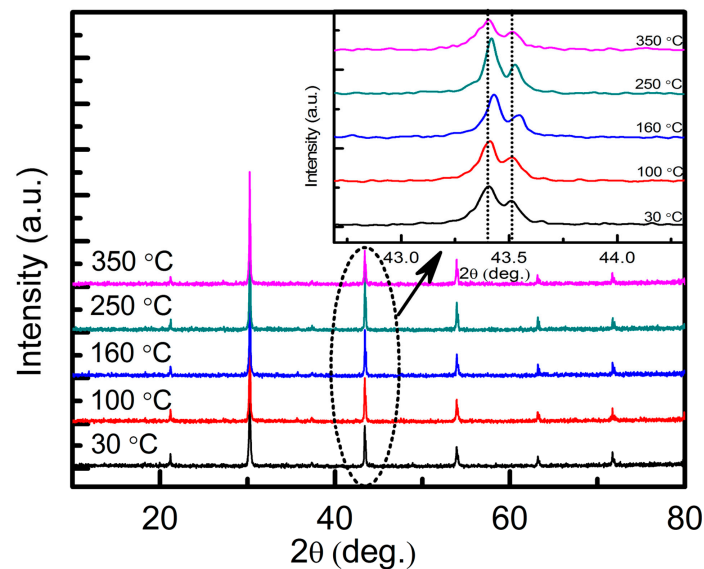


**Figure 9.** Temperature dependence of powder X-ray diffraction patterns of the crashed PLN-0.07PT crystal. The insert shows the (200) reflections.

## 5. Conclusions

Single crystals  $\text{Pb}(\text{Lu}_{1/2}\text{Nb}_{1/2})\text{O}_3\text{-PbTiO}_3$  with low PT (PLN-0.07PT) with a tetrakaidecahedron combination were successfully grown. The crystal structure was found to be orthorhombic in nature as revealed by the analysis of the XRD data. Both XRD and TEM show the super-lattice reflections due to short-range ordering of B-site cations. Micro-domains of 1–2 nm in size have been found from TEM. The typical FE domains have also been found from PLM and the extinction angle further confirms the crystal structure to be orthorhombic. The temperature dependence of the polarization-electric field hysteresis loops from room temperature to 220 °C demonstrates that a precursor/intermediate

state (125–170 °C) occurs above the Curie temperature (125 °C). The precursor/intermediate state exhibiting pinched hysteresis loops was displayed above the Curie temperature, which originates from some polar region embedded in the non-polar matrix. These pinched hysteresis loops possessing electric dipoles are intrinsic in nature and occur from the temperature  $T_{PR} = 1.1 * T_C$  (443 K). Another feature of PLN-0.07PT single crystals is that the Curie temperature of PLN-0.07PT is much lower than that of PLN and PT, which is related to the coexistence of the domains of the FE and AFE phases in a wide temperature range. The studies of phase transition PLN-0.07PT single crystal done here are a supplementary amendment of the PLN-PT phase diagram as previously reported. The investigations on a PLN-0.07PT single crystal not only help us to understand the binary PLN-PT system, but also to improve the potential applications of antiferroelectric PLN-based crystal. The transition between ferroelectric and antiferroelectric makes the application of PLN-based crystal more extensive.

**Acknowledgments:** This work was supported by the National Natural Science Foundation of China under Grant Nos. 51602308, 11404331, 91422303, and 11504373, the Science and Technology Project of Fujian Province under Grant No. 2015H0049, and the “Chunmiao” Talents Program for Young Scientists of the Haixi Institute of Chinese Academy of Sciences (CMZX-2016-006). C. He thanks V. M. Ishchuk (Inst. for Single Crystals of Acad. Sci. of Ukraine, Kharkov, Ukraine) and Alexei A. Bokov (Simon Fraser University, Canada) for discussion.

**Author Contributions:** Y.L. and X.Y. contributed to the experiment, the data analysis, and manuscript preparation. X.L. and Z.W. contributed to analysis and manuscript preparation. C.H. and X.L. conceived and designed the study. C.H. reviewed and edited the manuscript. All authors read and approved the manuscript.

**Conflicts of Interest:** The authors declare no conflict interest.

## References

1. Kittle, C. Theory of antiferroelectric crystals. *Phys. Rev.* **1951**, *82*, 729–732. [[CrossRef](#)]
2. Liu, Y.; Yang, X.; He, C.; Li, X.; Wang, Z.; Xiao, Y.; Long, X. Domain and antiferroelectric properties of  $\text{Pb}(\text{Lu}_{1/2}\text{Nb}_{1/2})\text{O}_3$  single crystals and their superlattice structure. *RSC Adv.* **2017**, *7*, 3704–3712. [[CrossRef](#)]
3. Parui, J.; Krupanidhi, S.B. Dielectric properties of (110) oriented  $\text{PbZrO}_3$  and La-modified  $\text{PbZrO}_3$  thin films grown by sol-gel process on Pt(111)/Ti/SiO<sub>2</sub>/Si substrate. *J. Appl. Phys.* **2006**, *100*. [[CrossRef](#)]
4. Park, Y.; Cho, K. Dielectric-state analysis in solid-solution  $\text{Pb}(\text{Yb}_{1/2}\text{Ta}_{1/2})\text{O}_3$ - $\text{Pb}(\text{Lu}_{1/2}\text{Nb}_{1/2})\text{O}_3$ . *J. Am. Ceram. Soc.* **2000**, *83*, 135–140.
5. Berlincourt, D.; Jaffe, H.A.; Krueger, H.H. Release of electric energy in  $\text{PbNb}(\text{Zr},\text{Ti},\text{Sn})\text{O}_3$  by temperature and by pressure-enforced phase transitions. *Appl. Phys. Lett.* **1963**, *3*, 90–93. [[CrossRef](#)]
6. Kupriyanov, M.F.; Fesenko, E.G. Investigation of the phase transition in  $\text{PbBI}_{0.5}\text{-BII}_{0.5}\text{O}_3$  compounds. *Bull. Acad. Sci. USSR Phys. Ser. (Engl. Transl.)* **1965**, *29*, 930–934.
7. Isupov, V.A.; Krainik, N.N. New antiferroelectrics having perovskite-type structure, containing rare-earth ions in octahedral lattice sites. *Sov. Phys.-Solid State USSR* **1965**, *6*, 2975–2976.
8. Zhang, Y.; Liu, P.; Chen, X.M.; Wu, J.L.; Yang, J.N. Effect of Ti on dielectric and piezoelectric properties of  $(\text{Pb}_{0.985}\text{La}_{0.01})_{1+y}(\text{Nb}_{1-y}\text{Ti}_y)_2\text{O}_6$  ceramics. *Mater. Des.* **2010**, *31*, 4886–4890. [[CrossRef](#)]
9. Park, S.E.; Markowski, K.; Yoshikawa, S.; Cross, L.E. Effect on electrical properties of barium and strontium additions in the lead lanthanum zirconate stannate titanate system. *J. Am. Ceram. Soc.* **1997**, *80*, 407–412. [[CrossRef](#)]
10. Sternberg, A.; Shebanovs, L.; Antonova, M.; Livinsh, M.; Yamashita, J.Y.; Shombalko, L.; Spule, A. New high piezoelectric coupling PLuNT binary system ceramics. *NanoStruct. Mater.* **1999**, *12*, 645–648. [[CrossRef](#)]
11. Antonova, M.; Shebanovs, L.; Livinsh, M.; Yamashita, J.Y.; Sternberg, A.; Shorubalko, I.; Spule, A. Structure and properties of hot-pressed  $\text{Pb}(\text{Lu}_{1/2}\text{Nb}_{1/2})\text{O}_3$ - $\text{PbTiO}_3$  binary system ceramics. *J. Electroceram.* **2000**, *4*, 179–187. [[CrossRef](#)]
12. Shen, D.; Li, X.; Wang, Z.; Liu, Y.; He, C.; Li, T.; Tailor, H.; Long, X. Preparation and characterization of  $(1-x)\text{Pb}(\text{Lu}_{1/2}\text{Nb}_{1/2})\text{O}_3-x\text{PbTiO}_3$  binary ferroelectric ceramics with high Curie temperature. *Mater. Lett.* **2012**, *84*, 1–4. [[CrossRef](#)]
13. Liu, Y.; Li, X.; Wang, Z.; He, C.; Li, T.; Ai, L.; Chu, T.; Pang, D.; Long, X. A new  $(1-x)\text{Pb}(\text{Lu}_{1/2}\text{Nb}_{1/2})\text{O}_3-x\text{PbTiO}_3$  binary ferroelectric crystal system with high Curie temperature. *CrystEngComm* **2013**, *15*, 1643–1650. [[CrossRef](#)]

14. Liu, Y.; Long, X. Growth and characterization of a new lead lutetium niobate with lead titanate ferroelectric crystal. *J. Inorg. Mater.* **2014**, *29*, 47–51. [[CrossRef](#)]
15. Liu, Y.; Yang, X.; Lai, F.; Huang, Z.; Li, X.; Wang, Z.; He, C.; Lin, J.; Long, X. Structure and properties of  $\text{Pb}(\text{Lu}_{1/2}\text{Nb}_{1/2})\text{O}_3\text{-}0.2\text{PbTiO}_3$  relaxor ferroelectric crystal. *Mater. Res. Bull.* **2015**, *67*, 83–86. [[CrossRef](#)]
16. Sawaguchi, E. Ferroelectricity versus antiferroelectricity in the solid solutions of  $\text{PbZrO}_3$  and  $\text{PbTiO}_3$ . *J. Phys. Soc. Jpn.* **1953**, *8*, 616–629. [[CrossRef](#)]
17. Xia, Z.; Li, Q. Phase transformation in  $(0.90 - x)\text{Pb}(\text{Mg}_{1/3}\text{Nb}_{2/3})\text{O}_3 - x\text{PbTiO}_3 - 0.10\text{PbZrO}_3$  piezoelectric ceramic: X-ray diffraction and Raman investigation. *Solid State Commun.* **2007**, *142*, 323–328. [[CrossRef](#)]
18. Rojac, T.; Drnovsek, S.; Bencan, A.; Malic, B.; Damjanovic, D. Role of charged defects on the electrical and electromechanical properties of rhombohedral  $\text{Pb}(\text{Zr,Ti})\text{O}_3$  with oxygen octahedral tilts. *Phys. Rev. B* **2016**, *93*. [[CrossRef](#)]
19. Rojac, T.; Kosec, M.; Budic, B.; Setter, N.; Damjanovic, D. Strong ferroelectric domain-wall pinning in  $\text{BiFeO}_3$  ceramics. *J. Appl. Phys.* **2010**, *108*. [[CrossRef](#)]
20. Srivastava, N.; Weng, G.J. A theory of double hysteresis for ferroelectric crystals. *J. Appl. Phys.* **2006**, *99*. [[CrossRef](#)]
21. Xu, B.; Paillard, C.; Dkhil, B.; Bellaiche, L. Pinched hysteresis loop in defect-free ferroelectric materials. *Phys. Rev. B* **2016**, *94*. [[CrossRef](#)]
22. Ko, J.-H.; Gorny, M.; Majchrowski, A.; Roleder, K.; Bussmann-Holder, A. Mode softening, precursor phenomena, and intermediate phases in  $\text{PbZrO}_3$ . *Phys. Rev. B* **2013**, *87*. [[CrossRef](#)]
23. Bussmann-Holder, A.; Beige, H.; Völkel, G. Precursor effects, broken local symmetry, and coexistence of order-disorder and displacive dynamics in perovskite ferroelectrics. *Phys. Rev. B* **2009**, *79*. [[CrossRef](#)]



© 2018 by the authors. Licensee MDPI, Basel, Switzerland. This article is an open access article distributed under the terms and conditions of the Creative Commons Attribution (CC BY) license (<http://creativecommons.org/licenses/by/4.0/>).